Reliability of Sharrocks equation for exchange spring bilayers

D. Suess,* S. Eder, J. Lee, R. Dittrich, and J. Fidler
Institute of Solid State Physics, Vienna University of Technology, Vienna, A-1040 Austria

J. W. Harrell
MINT Center and Department of Physics and Astronomy, University of Alabama, Tuscaloosa, Alabama 35487–0209, USA

T. Schrefl and G. Hrkac
Department of Engineering Materials, The University of Sheffield, Sheffield, S-10 2TN United Kingdom

M. Schabes, N. Supper, and A. Berger
San Jose Research Center, Hitachi Global Storage Technologies, San Jose, California 95135, USA
(Received 19 January 2007; published 22 May 2007)

A Monte Carlo approach and a modified nudged elastic band method are used to study the dynamic coercivity of interacting particle arrays in particular perpendicular recording media and exchange spring bilayers. Monte Carlo simulations are performed to study the effect of the interactions on the dynamic coercivity of interacting particle arrays. It is shown that the interactions in magnetic recording media only slightly influence the dynamic coercivity. The reliability of energy barrier measurements based upon Sharrock's equation for frequency-dependent coercivity data is investigated using a modified nudged elastic band method. It is shown that the extrapolated energy barrier at zero field may deviate from the correct one by up to 18% if the conventional exponent $n=1.5$ is assumed. Our micromagnetic simulations furthermore indicate that the accuracy of the extrapolated energy barrier can be improved by about a factor of 3 upon measuring the dynamic coercivity at an angle of 45° and using the exponent n as an additional fit parameter.

DOI: 10.1103/PhysRevB.75.174430 PACS number(s): 74.25.Ha

I. INTRODUCTION

With increasing areal density in magnetic recording, new concepts have to be introduced in order to obtain a high thermal stability and a good writeability and, at the same time, a good signal-to-noise ratio. For example, a breakthrough technology in longitudinal recording was introduced with the concept of antiferromagnetic coupled (AFC) media.[1,2] Recently, perpendicular recording was introduced into products, which allows a further increase in areal density. With increasing areal density the grains in the recording media have to be decreased in diameter. However, in the most simple picture where the thermal stability depends on the volume of one grain, a minimum volume is required to obtain the required thermal stability. In future perpendicular recording media it will be a trade-off between areal density and thermal stability. Therefore it is important to be able to measure the thermal stability of advanced magnetic recording media with high accuracy. The lifetime of stored information (thermal stability) in granular recording media is obviously connected to the stability of the magnetization states in each grain, which can be estimated by the Arrhenius-Néel formula

$$\tau = \tau_0 e^{\Delta E/k_B T}. \quad (1)$$

Here, ΔE is the energy barrier which separates the two magnetic lowest-energy states in a recording media grain. τ_0 is the inverse of the attempt frequency. A commonly used method to determine this energy barrier as well as the short-time coercive field (switching field) H_0 of longitudinal recording media was proposed by Sharrock.[3] More recently, the validity of Sharrock's equation for more complex magnetic recording materials, such as AFC media was investigated by Margulies *et al.*[4]

In this paper the validity of Sharrock's equation for the case of perpendicular recording media and, more specifically, for the case of exchange spring media is investigated. Exchange spring media consist of strongly-exchange-coupled hard and soft layers. Exchange spring magnets were initially introduced by Coehoorn *et al.*[5] and Kneller and Harwig[6] for permanent magnet applications. The optimal tuning of the fraction of the soft magnetic phase and the hard magnetic phase allowed the design of materials with a high remanence and at the same time a high coercive field.[7] Experiments on exchange spring films, in particular on a bilayer structure consisting of a soft magnetic NiFe layer, coupled to a CoSm layer, were done by Mibu *et al.*[8] and Fullerton *et al.*[9] for the scope of a high-energy product for hard magnetic materials.

Recently, the compositions of hard and soft magnetic layers were introduced theoretically[10,11] to reduce the write field requirements in magnetic recording. Experimental work on exchange spring media was done by Wang *et al.*[12] and Supper *et al.*[13] The influence of the interface coupling on the coercive field and the compression of the domain wall at the hard-soft interfaces can be found in Refs. 14–17.

In a multilayer structure with continuously increasing anisotropy from layer to layer it was shown theoretically that the coercive field can be decreased to an arbitrarily small value while keeping the energy barrier (thermal stability) constant.[18]

Studies of exchange spring structures show that extremely hard magnetic films can be written with a limited head field if they are coupled to softer magnetic layers. Interestingly

the scope of exchange spring media (ESM) in magnetic recording is opposite to the scope of exchange spring magnets for permanent magnets. In magnetic recording ESM should drastically decrease the coercive field, while it should be maintained high in permanent magnet applications.

The paper is structured as following. In Sec. II the basic concept of measuring the thermal stability using Sharrock's equation is given. In Sec. III micromagnetic models are discussed that allow one to simulate magnetic structures at finite temperature. In particular the introduction of a Monte Carlo method is given that allows one to simulate the hysteresis loop of recording media at finite temperature. Furthermore, Sec. III deals with the nudged elastic band method, which allows for the calculation of energy barriers of magnetic structures.

In Sec. IV validation of Sharrock's equation is investigated for perpendicular recording media and exchange spring media. First, the effect of the interactions field is investigated using the Monte Carlo method introduced in the previous section. Finally, energy barrier calculations on a single grain of various exchange spring media are performed.

II. BACKGROUND OF SHARROCK's EQUATION

Let us start with a quick review of Sharrock's equation. In the following it is assumed that each grain of the recording system can be described by a two-level system. One level corresponds to the state with magnetization up; the other level corresponds to the state with magnetization down. One is interested in the average lifetime of the state with magnetization pointing up. The occupation probabilities of the two energy levels P_1 and P_2 satisfy the normalization condition $P_1+P_2=1$ and the master equation $\frac{dP_1}{dt}=-w_{12}P_1+w_{21}P_1$, where w_{12} is the transition rate from the up state to the down state and w_{21} the transition rate from the down to the up state. w_{12} is the inverse of the average lifetime of the up state, $w_{12}=\frac{1}{\tau}$. The magnetization as a function of time, which depends on the occupation probability P_1 and P_2, can be written as

$$M(t)=M_s(P_1-P_2)=M_s(2P_1-1). \tag{2}$$

For sufficiently large downward fields the up state has a much larger energy than the down state. In this limit w_{21} is much smaller than w_{12} and can be set to zero. Under this assumption, it follows that $P_1=e^{-w_{12}t}$.

For macroscopic particle assemblies, such as recording media, in an accurate approach the energy barrier has to be replaced by a distribution of energy barriers, which results in the fact that the decay of the magnetization no longer follows an exponential decay. Instead, one finds that for a distribution of energy barriers the magnetization decreases according to a logarithmic law as a function of time.[19]

In the following the simple case of only one energy barrier height is investigated. The average life time τ can be extracted by substituting the equation for P_1 into the equation for $M(t)$ and calculating the time t_0, when $M(t_0)=0$. It follows that $t_0=\tau\ln(2)$. Therefore, applying a field and measuring the time t_0 until the magnetization becomes zero allows one to determine τ, which depends on the system, particularly on the energy barrier separating the state up from the state down. From the measurement of the time τ the energy barrier can be extracted using Eq. (1). However, the energy barrier of recording media at zero field cannot be extracted from τ, because the average lifetime τ for media is usually several years and cannot be accessed experimentally. A way to enhance the decay of the magnetization is to apply an external field that opposes the magnetization. From the decay of the magnetization at finite fields one tries to estimate the thermal stability at zero field. For Stoner-Wohlfarth particles the energy barrier at finite opposing field is connected to the energy barrier at zero field by the relation

$$\Delta E=\Delta E_0\left(1-\frac{H}{H_0(\theta)}\right)^n, \tag{3}$$

where $H_0(\theta)$ is the Stoner-Wohlfarth switching field, when the external field is applied at an angle θ with respect to the anisotropy axis. Upon applying the external field exactly parallel to the easy axis, the exponent n is found to be 2. However, the exponent will deviate significantly if $\theta>0$. Victora expressed the energy barrier as a series expansion as $\Delta E=C_1(1-H/H_0)^{3/2}+O(5/2)$.[20] Harrell investigated in detail the exponent n as a function of the external field H and the angle between the external field and the easy axis of single domain particles.[21] He found that for an angle $\theta=15.9°$ the exponent n is very close to 1.5 for all external field values. For $\theta=1°$ the exponent depends on the external field and decreases from 1.85 to 1.62 as the external field increases from zero to the coercive field. For $\theta=45°$ the value of the exponent n is between 1.4 and 1.5. For the analysis of experiments, different values of the exponent n are used, such as $n=2$ (Ref. 22) and $n=3/2$ (Ref. 23).

Substituting the Arrhenius-Néel formula into Eq. (3) leads to Sharrock's equation

$$H_{c,dyn}=H_0\left\{1-\left[\frac{k_BT}{\Delta E_0}\ln\left(\frac{t_0}{\ln(2)\tau_0}\right)\right]^{1/n}\right\}. \tag{4}$$

Therefore applying different external fields $H_{c,dyn}$ and measuring for every field the time t_0 until the magnetization becomes zero allows one to determine ΔE_0 and H_0. This procedure is usually called measuring the time dependence of the coercivity.

III. MICROMAGNETIC THEORY

A. Energy barriers

In magnetic storage applications thermal switching events determine the long-term stability of the stored information. The main difficulty in the computation of transition processes is caused by the disparity of the time scales. If the thermal energy k_BT is comparable to the energy barrier ΔE separating two local energy minima, direct simulations of the escape over the energy barrier using Langevin equation are possible.[24,25] However, this is usually not the case in magnet recording applications where $k_BT\ll\Delta E$. Due to the granularity in magnetic recording simulations, it is a good approximation that switching occurs grain by grain. Therefore, the

thermal stability can be estimated if the energy barrier of each grain is known.

Henkelman and Jónsson proposed the nudged elastic band method to calculate minimum-energy paths.[26] A path of the nudged elastic band method is represented by a sequence of images. One image represents one magnetization state of the magnetic system. An initial path is assumed which connects the initial magnetization state $\mathbf{M}^{(i)}$ with the final magnetization state $\mathbf{M}^{(f)}$.

In the work of Henkelman and Jónsson chemical processes are simulated. Therefore the coordinates of the nudged elastic band method denote the position of particles. In contrast to space coordinates, the magnetization in micromagnetics has to fulfill the constraint that the magnitude remain constant with time. Therefore it is not possible to directly use the formulation of the nudged elastic band method as proposed by Henkelman and Jónsson. Dittrich *et al.* successfully applied the nudged elastic band to micromagnetics using polar coordinates in order to fulfill the constraint of a constant magnetization.[27] However, convergence problems can occur because of the problem of a good definition of the difference vector between two magnetization states in polar coordinates. The difference vector is required in the nudged elastic band method in order to relax the initial path towards the minimum-energy path.

In order to avoid this problem the magnetization of the nudged elastic band method is represented by Cartesian coordinates in the following. A modified relaxation procedure in the nudged elastic band method is proposed. Every image consists of M discretization points (e.g., node points of the finite-element mesh or cells of a finite-difference scheme).

On each discretization point the magnetic polarization is described by a three-dimensional vector. The magnetization of the image i and the discretization point k is given by

$$\mathbf{J}_{i,k} = (J_x, J_y, J_z). \tag{5}$$

The optimal path can be found by solving the following partial differential equation for the magnetization $\boldsymbol{J}_{i,k}$ on every node point on each image:

$$\frac{\partial \mathbf{J}_{i,k}}{\partial t} = -\frac{|\gamma|}{J_s}\mathbf{J}_{i,k} \times [\mathbf{J}_{i,k} \times \mathbf{D}_{i,k}(\mathbf{J})]. \tag{6}$$

The three-dimensional vector $D_{i,k}$ can be regarded as an effective field. The right-hand side of Eq. (6) has the same form as the damping term of the Landau-Lifshitz-Gilbert equation. As a consequence Eq. (6) conserves the magnitude of the magnetization in time. The vector $\mathbf{D}_i$ is composed of three-dimensional vectors $\mathbf{D}_{i,k}$ on every discretization point of each image i,

$$\mathbf{D}_i = (\mathbf{D}_{i,1}, \mathbf{D}_{i,2}, \ldots, \mathbf{D}_{i,M}). \tag{7}$$

This vector, which governs the relaxation of the images towards the minimum-energy path, is calculated using Eq. (8),

$$\mathbf{D}_i = \{\mathbf{H}_{eff,i}(\mathbf{J}_i) - (\mathbf{H}_{eff,i}(\mathbf{J}_i) \cdot \mathbf{t}_i)\mathbf{t}_i\} + \mathbf{F}_i. \tag{8}$$

The effective field is the negative functional derivative of the total Gibbs' energy density of the image i,

$$\mathbf{H}_{eff,i} = -\frac{\delta \varepsilon_{Gibb}}{\delta \mathbf{J}} = \frac{2A}{J_S}\Delta \mathbf{J}_i + \frac{2K_u}{J_S^2}(\mathbf{J}_i \cdot \mathbf{u})\mathbf{u} + \mathbf{H}_S + \mathbf{H}_{ext}. \tag{9}$$

The first term denotes the exchange energy contribution with A as the exchange constant. The second term is the anisotropy term with K_u as the magnetocrystalline anisotropy constant and $\mathbf{u}$ the unitary direction vector of the easy magnetization axis. $\mathbf{H}_S$ and $\mathbf{H}_{ext}$ are the stray field and the external field, respectively.

Care has to be taken when calculating the local tangent t_i at an image i. The single use of either a forward-difference approximation, backward-difference approximation, or a central-difference approximation develops kinks in the path.[26] The kinks prevent the string from converging to the minimum-energy path. The optimal choice of the appropriate difference approximation depends on the energy difference between successive images. In a first approach, forward differences climbing up a hill, backward differences going down a hill, and central differences at energy minima and maxima are used. The tangent $\mathbf{t}_i$ can be calculated using

$$\mathbf{t}_i = \frac{\mathbf{J}_{i+1} - \mathbf{J}_i}{\|\mathbf{J}_{i+1} - \mathbf{J}_i\|} \quad \text{if } E(\mathbf{J}_{i-1}) < E(\mathbf{J}_i) < E(\mathbf{J}_{i+1}), \tag{10}$$

$$\mathbf{t}_i = \frac{\mathbf{J}_i - \mathbf{J}_{i-1}}{\|\mathbf{J}_i - \mathbf{J}_{i-1}\|} \quad \text{if } E(\mathbf{J}_{i-1}) > E(\mathbf{J}_i) > E(\mathbf{J}_{i+1}), \tag{11}$$

$$\mathbf{t}_i = \frac{\mathbf{J}_{i+1} - \mathbf{J}_{i-1}}{\|\mathbf{J}_{i+1} - \mathbf{J}_{i-1}\|} \quad \text{if } E(\mathbf{J}_{i-1}) < E(\mathbf{J}_i) > E(\mathbf{J}_{i+1})$$

$$\text{or if } E(\mathbf{J}_{i-1}) > E(\mathbf{J}_i) < E(\mathbf{J}_{i+1}). \tag{12}$$

This prevents the formation of kinks. A detailed analysis of this topic and the motivation for this choice of the tangent can be found in the work of Henkelman and Jónsson.[26] The norm which is used in all expressions is the L^2 norm.

The last term of Eq. (8) denotes the spring force. It prevents the images from moving towards the end points and local minima of the path, giving a low resolution near saddle points and a high resolution near energy minima. This problem is known as "sliding-down" and can be solved by introducing spring forces between the images which make them stay equally spaced in the L^2 norm:

$$\mathbf{F}_i = \frac{k}{\mu_0}(\|\mathbf{J}_{i+1} - \mathbf{J}_i\| - \|\mathbf{J}_i - \mathbf{J}_{i-1}\|)\frac{\boldsymbol{\tau}_i}{\|\boldsymbol{\tau}_i\|}. \tag{13}$$

The direction of the spring force is given by the difference of the magnetization state of two images,

$$\boldsymbol{\tau}_k^+ = \mathbf{J}_{k+1} - \mathbf{J}_k, \tag{14}$$

$$\boldsymbol{\tau}_k^- = \mathbf{J}_k - \mathbf{J}_{k-1}, \tag{15}$$

$$\boldsymbol{\tau}_k = \boldsymbol{\tau}_k^+ \quad \text{if } E(\mathbf{J}_{k-1}) < E(\mathbf{J}_k) < E(\mathbf{J}_{k+1}), \tag{16}$$

$$\boldsymbol{\tau}_k = \boldsymbol{\tau}_k^- \quad \text{if } E(\mathbf{J}_{k-1}) > E(\mathbf{J}_k) > E(\mathbf{J}_{k+1}). \tag{17}$$

One problem is the choice of the strength of the spring constant k. The optimal value for k depends on the number of images used, on the number of finite elements, and on the size of the model. It is difficult to give a general rule for the value of the spring constant. It should be strong enough to prevent images from falling down into the energy minima, but not too strong as to dominate by orders of magnitude in Eq. (8). Fortunately, the absolute value of k is usually not very critical and can be varied over several orders of magnitude without losing speed within the time integration scheme.

B. Monte Carlo simulations

The nudged elastic band method is a powerful tool to estimate the thermal stability for systems with small numbers of energy minima and saddle points. However, for calculation of the magnetization decay of a granular recording media the sole application of the nudged elastic band method does not provide the magnetization as a function of time or field. For these systems a better approach is the use of Monte Carlo methods. Bortz *et al.* investigated activated reversal processes of Ising spin systems with Monte Carlo methods.[28] Charap *et al.* used Monte Carlo methods in order to estimate the areal density limit of longitudinal recording.[29] The time increment in the Monte Carlo method was adjusted according to the average time between successful reversals. Therefore the method could describe magnetization reversal processes of any time span of interest. However, the method used by Charap *et al.* is not suitable to calculate hysteresis loops with different field sweep rates. Chantrell *et al.* used a Monte Carlo method to model the low-field susceptibility of a cobalt granular system.[30] Standard Monte Carlo steps are performed in order to achieve a correct thermodynamic description of the magnetization states close to an energy minimum. In order to model thermal activations over larger energy barriers the Arrhenius-Néel model is applied. For each grain of the recording media the probability of switching within the measuring time t_m (time step of the Monte Carlo method) is given by

$$P_r = 1 - e^{-t_m/\tau}, \tag{18}$$

where τ is the relaxation time given by Eq. (1). The Monte Carlo simulations performed in this paper are based on the work by Chantrell *et al.* A granular microstructure was constructed using Voronoi tessellations. The equilibrium magnetization state is described with one magnetic polarization vector. For every magnetization state the finite-element method is used to calculate the effective field on every grain of the media. The effective field contains the demagnetizing field of the neighboring grains, the exchange field, and the external field. For the Monte Carlo method one grain i of the media is chosen at random. The switching probability within the time step t_m was calculated according to Eq. (18). On average all grains are chosen one time within the time t_m. In the following simulations the time step t_m was chosen sufficiently small that the results do not depend on t_m. The energy barrier in Eq. (18) depends on the effective field acting on grain i. In order to calculated the energy barrier two different approached are used. In the first approach we followed the work of Chantrell *et al.*[30] The energy barrier is calculated using the Pfeiffer approximation.[31] In the second approach the energy barriers for the system were precomputed using the nudged elastic band method. In order to calculate the energy barriers for an arbitrary grain i of the media the following procedure was applied. A finite-element model was constructed to model a standard grain with a basal plane of 1 nm$\times$1 nm and a thickness that equals the film thickness. The obtained energy barrier was multiplied by the area of the basal plane of the grain i. In order to save computational time in a preprocessing step a table was constructed that contains the energy barrier for discrete values of the effective field and the angle θ between the external field and the easy axis. For every field value and angle θ the energy barrier was calculated using the nudged elastic band method as described in the previous section. Figure 1 compares the precomputed energy barriers using the nudged elastic band method with the Pfeiffer approximation for a grain with a rectangular basal plane with an edge length of 1 nm. The film thickness is 20 nm, the anisotropy constant $K_1 = 3 \times 10^5$ J/m^3, and the exchange constant $A = 10^{-11}$ J/m. The magnetic polarization $J_s = 0.5$ T. The demagnetizing field of the grain which leads to a shape anisotropy was not taken into account. For the precomputed barriers the external field was discretized between zero and the switching field using 20 mesh points. The angle θ was discretized between 0 and 90° using 14 discretization points. Figure 1 shows that the Pfeiffer approximation is well suited to estimate the energy barriers even for a grain with a thickness of 20 nm.

For the Monte Carlo simulation a second-order interpolation scheme was used to evaluate the energy barrier for any arbitrary point $E(H, \theta)$. This method allows for the calculation of the thermal stability of recording structures where the thermally activated reversal mechanism occurs via a formation of a nucleation. This is particularly important for exchange spring media.

IV. MICROMAGNETIC RESULTS

A. Monte Carlo simulations of single-phase media

Sharrock's equation [Eq. (4)] was derived under the assumption that no interaction fields act on the media. However, if the time-dependent coercivity is measured for a granular recording media, this assumption may not be justified. The internal field that acts on one grain changes during the measurement. At the beginning of the measurement all grains point up. The full demagnetizing field adds to the external field. At $M_z = 0$ the demagnetizing field is zero (at least within the mean-field approximation), leading to zero demagnetizing field. However, the field $H_{c,dyn}$ in Eq. (4) is assumed to be constant. If the external field is applied at a finite angle with respect to the film normal, apart from the magnitude of the internal field, also the angle of the internal field changes during the measurement. A similar problem occurs if the intrinsic hysteresis loop of a tilted recording medium is measured. The internal field angle (sum of the

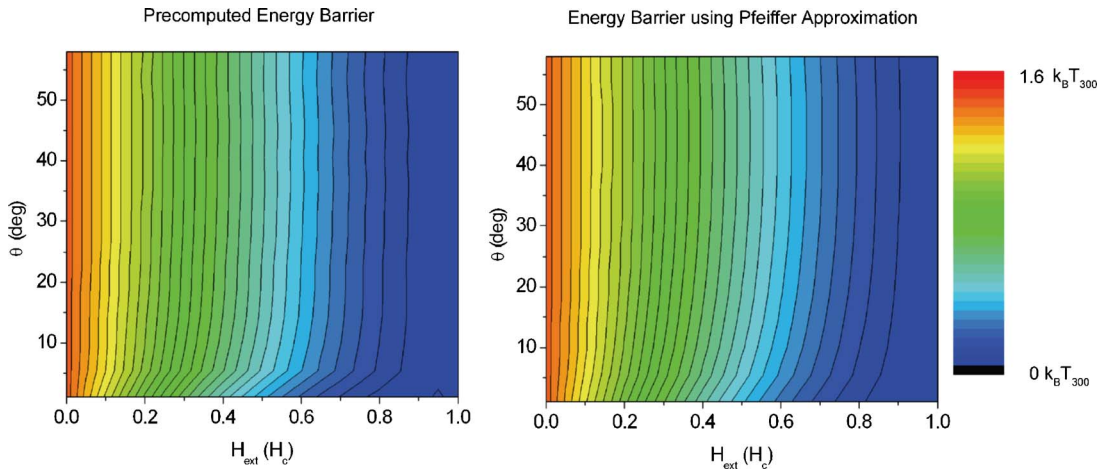

FIG. 1. (Color online) Energy barrier as a function of the external field and the angle θ between the easy axis and the external field. The grain has a rectangular basal plane with edge length of 1 nm. The film thickness is 20 nm. Left image: the energy barrier was calculated using the nudged elastic band method. The barrier is calculated for 20 different values of the external field and 14 values of the angle θ. Right image: the Pfeiffer approximation is used to estimate the energy barrier.

external field, the exchange field, and the demagnetizing field) changes along the hysteresis loop even if the angle of the applied field is kept constant. This problem was discussed by Richter who suggested an iterative procedure to compensate for the error.[32] Recently, the iterative procedure was used to measure intrinsic hysteresis loops of perpendicular recording media at different angles between the easy axis and the film normal.[33]

In order to investigate the influence of the interaction field on the dynamic coercivity, Monte Carlo simulations as described in Sec. III are performed. A recording media with 20×20 grains is simulated. The grain diameter is 6.5 nm and the film thickness is 20 nm. The magnetic polarization is 0.5 T and the exchange constant is $A=10^{-11}$ J/m. The anisotropy constant is $K_1=3\times 10^5$ J/m^3. No distribution of the easy axis is assumed in order to clearly separate the effect of the interaction field on the dynamic coercivity. The external field is applied at an angle of 15.9° with respect to the easy axis. In a first set of simulations the exchange field and the stray field were not taken into account. The dashed lines in Fig. 2 show the remanent hysteresis loops for different waiting times t at a temperature of $T=300$ K. The remanent hysteresis loops are obtained by first saturating the sample. An external field H is applied for a time t. After the time t the field is removed and the remanence is measured. This is done for different fields H in order to obtain the remanent hysteresis loop. The different dashed curves in Fig. 2 denote simulations for different waiting times t.

The numerically obtained values of the dynamic coercivity are plotted as a function of $\ln(\kappa t)$ in Fig. 3. t is the waiting time and $\kappa=1/[\tau_0 \ln(2)]$, where $\tau_0=10^{-9}$ s. The curves in Fig. 3 are fitted using Eq. (3) in order to determine the energy barrier ΔE_0 and H_0. Equivalently the energy barrier ΔE_0 and H_0 can be obtained by fitting $H(\ln(\kappa,t))$ data to Sharrock's equation. Equation (3) is the inverse function of Sharrock's equation.

For the simulations neglecting the demagnetizing field and the exchange field the dynamic coercivities (circles in Fig. 3) agree very well with the values obtained from Sharrock's equation (solid line in Fig. 3). ΔE_0 and H_0 in Sharrock's equation were calculated using the micromagnetic input parameters. The differences between the analytically obtained dynamic coercive fields (from Sharrock's equation) and the numerical values were smaller than 10^{-3} T ($<0.4\%$) for all simulations.

The numerical obtained curves of Fig. 3 were fitted with Sharrock's equation in order to obtain the energy barrier ΔE and H_0. The exponent n in Eq. (19) was assumed to be $n=1.55$ which follows from the Pfeiffer approximation. As expected for zero interactions, the fitted values of ΔE and H_0 agree very well with the calculated ones. The fitted values are $\Delta E_{0,\mathrm{fitt}}=48.32k_BT_{300}$ and $\mu_0 H_{0,\mathrm{fitt}}=0.918$ T. The Stoner-

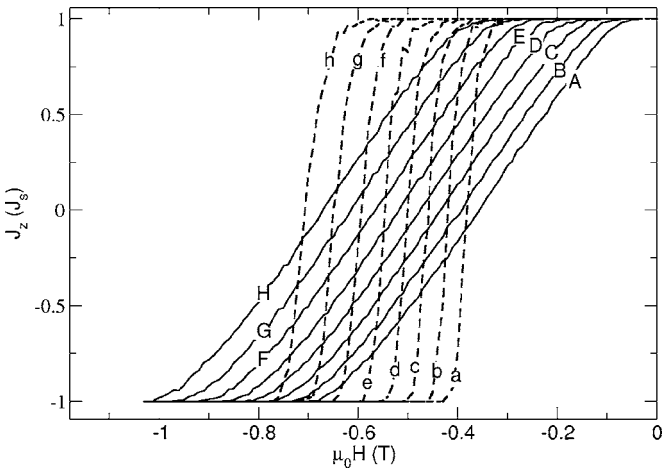

FIG. 2. Remanent hysteresis loops obtained by Monte Carlo simulations. The temperature $T=300$ K. No intergranular exchange field is assumed in the calculations. The waiting time is $t=1$ s, 10^{-1} s, 10^{-2} s, …, 10^{-9} s for the curves $a,b,c,\ldots,h$, respectively. The angle between the easy axis and the external field is 15.9°. Dashed lines a-h: the stray field of neighboring grains is not taken into account. Solid lines A-H: same as a-h but the demagnetizing field is taken into account.

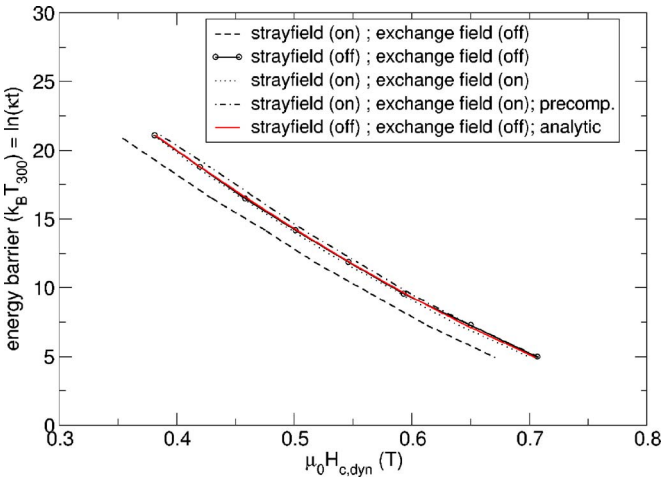

FIG. 3. (Color online) Compilation of the dynamic coercivity obtained from the waiting time experiments of Fig. 2. The temperature is $T=300$ K. Instead of the waiting time t the logarithm $\ln(\kappa t)$ is used as the y axis. The constant $\kappa=1/[\tau_0 \ln(2)]$. The effect of interaction fields (stray field and exchange field) on the dynamic coercivity is investigated.

Wohlfarth theory gives for the micromagnetic input parameters $\Delta E_{0,\mathrm{SW}}=48.7k_BT_{300}$ and $\mu_0 H_{0,\mathrm{SW}}=0.914$ T.

In order to investigate the influence of the stray field interactions, the simulations were repeated taking the demagnetizing field into account. The self-demagnetizing field of one grain of the recording media that leads to a shape anisotropy was not taken into account in order to be able to compare the results directly with the simulations where the demagnetizing field was neglected. The demagnetizing field leads to a small reduction of the dynamic coercive field as shown in Fig. 2 (solid lines) and Fig. 3 (dashed line). This is in contrast to a simple mean-field theory where at coercivity no mean field acts on the grains. Again Sharrock's equation was used to fit the numerical obtained values of the dynamic coercivity leading to $\Delta E_{0,\mathrm{fitt}}=46.47k_BT_{300}$ and $\mu_0 H_{0,\mathrm{fitt}}=0.88$ T.

Finally, simulations were performed taking into account the demagnetizing field and an exchange field between the grains with a mean exchange field of 0.16 T. Interestingly, the dynamic coercive field increases as the exchange interactions are introduced leading to $\Delta E_{0,\mathrm{fitt}}=48.8k_BT_{300}$ and $\mu_0 H_{0,\mathrm{fitt}}=0.9$ T as shown in Fig. 3 (dotted line).

In all previous simulations the energy barriers in the Monte Carlo simulations where calculated using the Pfeiffer approximation. Simulations with precomputed energy barriers using the nudged elastic band method are shown by the dotted dashed line in Fig. 3. The simulations show that for single-phase media and a film thickness of 20 nm the results only slightly deviate from the simulations using the Pfeiffer approximation (dotted line).

B. Energy barriers of bilayers with a perfectly soft layer

In the last section it was shown that an extrapolation using Sharrock's equation leads to values of H_0 and $\Delta E_{0,\mathrm{fitt}}$ that are not significantly influenced by the interaction fields. This can be understood by the following argument. The state of the film where the values of H_0 and $\Delta E_{0,\mathrm{fitt}}$ are measured (fitted) is the demagnetized state. Therefore, 50% of the grains are pointing up and the other 50% are pointing down, leading to zero mean field in first order. The measured $\Delta E_{0,\mathrm{fitt}}$ also has a physical meaning for magnetic recording. It approximates the energy barrier of a grain at the transition. At the transition it is justified to assume that no demagnetizing field and no exchange field (this is only true in the limit for weak exchange) act on the grain.

However, usually the most unstable grains in magnetic recording are the grains close to the center of a bit. Here, a large demagnetizing field acts on the grains. In order to estimate the thermal stability of a grain at the center of a bit, care has to be taken because the extrapolated value of $\Delta E_{0,\mathrm{fitt}}$ does not take demagnetizing fields into account. The influence of neighboring grains (demagnetizing field and exchange field) on the energy barrier in a saturated film is investigated in Ref. 17. It is shown that the influence of the demagnetizing field and the exchange field can be treated with a mean-field approach. $\Delta E_{0,\mathrm{fitt}}$ only corresponds to the energy barrier of a grain in the demagnetized film if the exponent n of the energy barrier as a function of the external field is known in detail. In order to calculate the exponent n for exchange spring media the energy barrier is calculated numerically using the nudged elastic band method. The exchange constant and the magnetic polarization are the same as in the last section. In contrast to the last section only one grain of the exchange spring media is modeled. This effective mean field can be added to the external field. The grain diameter of Fig. 4 shows the energy barrier as a function of the external field for exchange spring media with different soft layer thicknesses. If not stated otherwise, in all the simulations the following parameters are used. The magnetic polarization in the hard layer and the soft layer is $J_s=0.5$ T. The exchange constant $A=1\times10^{-11}$ J/m. The anisotropy in the hard layer is $K_1=1\times10^6$ J/m^3.

In Fig. 4 the external field is applied at an angle $\theta=0.5°$ with respect to the easy axis. In the limit of an infinitely thick soft and an infinitely thick hard magnetic layer an analytic expression for the energy barrier as a function of an applied field ($\theta=0$) was derived by Loxley and Stamps.[34] The predictions of the analytical formula are compared with values obtained from the nudged elastic band method for a soft-layer thickness of 36 nm and an angle θ of 0.5°. As shown in Fig. 4 the agreement is excellent, especially for values of the external field larger than about 0.5 times the dynamic coercive field. For large field values the external field strongly pushes the domain wall against the hard-soft interface, leading to a small width of the domain wall at the saddle point, which is the state along the minimum-energy path with the largest energy. In terms of the domain wall width, the external field can be thought of an effective anisotropy in the order of J_sH. For smaller field values, the width of the domain wall at the saddle point is larger than the thickness of the soft magnetic layer, leading to deviations from the analytical formula due to the finite soft-layer thickness.

Since Eq. (3) was derived for single-domain particles, it is not obvious at all if it can be used for exchange spring media where highly nonuniform states are formed during reversal.

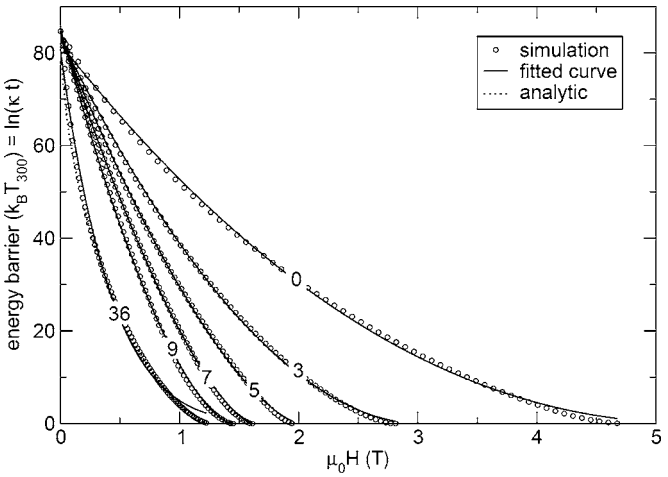

FIG. 4. Energy barrier of exchange spring media for different soft-layer thicknesses as a function of the external field strength. The grain diameter is 6 nm; the hard-layer thickness is 18 nm. The anisotropy constant in the hard layer is $K_{1,\mathrm{hard}}=1\times10^6$ J/m^3. The numbers in the plot (0–36) denote the soft-layer thickness in nm. The solid lines are fitted to numerically calculated energy barriers using E_0, H_0, and n as fit parameters. The angle between the easy axis and the external field is $\theta=0.5°$. The dotted line shows the results of the analytical formula that is valid for $\theta=0°$ and infinite thick layer thicknesses. Exchanging the x axis and the y axis in the above plot gives a curve which is usually called "time dependence of the remanent coercivity."

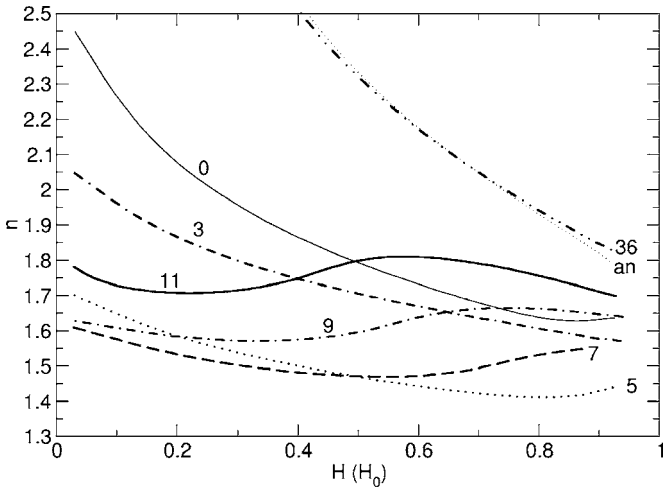

FIG. 5. Field dependence of the fitting parameter n. $\theta=0.5°$. The hard-layer thickness $t_h=18$ nm. The numbers next to the curves denote the soft-layer thickness.

In order to check whether Eq. (3) is valid or not, the exponent n is calculated as a function of the external field for various exchange spring media. Similar to experiments where the external field is applied perpendicular to the film plane, the exponent n is calculated for an angle θ of 0.5°. The exponent n is locally fitted in a field range of about 0.1 T (five data points). For the fit the numerically calculated values for ΔE and $H_0(\theta)$ are used.

Figure 5 shows that n strongly depends on the value of the external field. It is interesting to note that even the single-phase media without a soft layer show a nonconstant exponent n. This is different to the Stoner-Wohlfarth theory where the exponent n does not exceed a value of 2 (Ref. 21). The reason is that in the investigation the hard-layer thickness is 18 nm. Slightly inhomogeneous states are formed that lead to different results from the Stoner-Wohlfarth theory. Micromagnetic simulations of a sample with a thickness of 10 nm lead to very similar results as reported by Harrell.[21]

The numerical results for a soft layer thickness $t_s=36$ nm very well agree with the analytical results. The analytical formula[34] shows that in the limit of zero external field n goes towards infinity. Even for larger values of H the exponent n is significantly larger than 1.5. This indicates that an experimental fit with $n=1.5$ leads to significantly wrong results and that the energy barrier as a function of the exter-

TABLE I. Compilation of the error of the extrapolated energy barrier $\Delta E=E_{\mathrm{fitted}}-E_{\mathrm{real}}$ and the extrapolated H_0 using Sharrock's equation for different soft-layer thicknesses t_s. The thickness of the hard layer is 18 nm. $\theta=0.5°$. n_{global} is determined by fitting the exponent n with Sharrock's equation in the whole field range ($0<H<H_0$). In all other columns Sharrock's equation is fitted in the range $5k_BT_{300}<\Delta E(H)<20k_BT_{300}$. The columns "fit n" determine the error of H_0 and ΔE if n is used as a free fit parameter. The columns $n=1.5$ denote the error if n is set constant to 1.5 which is done in most experimental measurements. In the columns $n=n_{\mathrm{global}}$, H_0 and ΔE are determined from the fits using n_{global} of the second columns. In the last row the standard deviation is calculated of the six lines above.

		Error $\mu_0 H_0$ (T)			Error ΔE (k_BT_{300})		
t_s (nm)	n_{global}	Fit n	$n=1.5$	$n=n_{\mathrm{global}}$	Fit n	$n=1.5$	$n=n_{\mathrm{global}}$
0	1.90	−0.01	**−0.01**	0.21	−15.97	**−15.97**	−7.19
3	1.87	0.02	**−0.01**	0.08	−9.39	**−11.72**	−4.80
5	1.51	−0.04	**0.03**	0.01	−9.74	**2.68**	−0.61
7	1.47	−0.02	**−0.03**	−0.05	10.93	**6.91**	3.98
9	1.62	0.05	**−0.05**	−0.03	15.58	**−5.26**	0.28
11	1.78	0.07	**−0.06**	0.02	3.61	**−14.61**	−2.99
Standard deviation		0.04	**0.03**	0.09	12.72	**9.47**	3.96

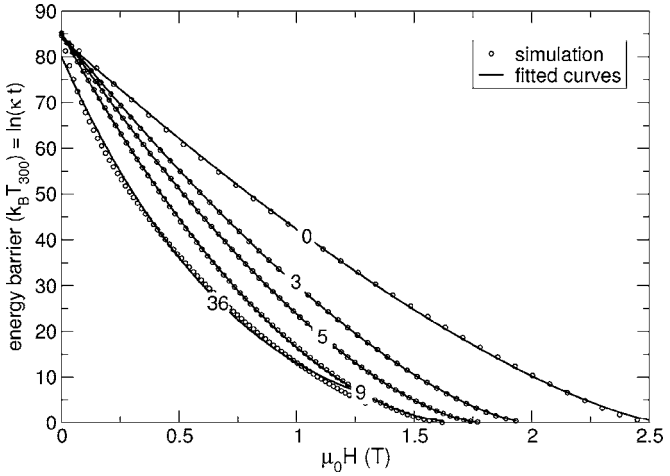

FIG. 6. Same as Fig. 4 except that the external field is applied at an angle of θ=45°.

nal field can hardly be described by Eq. (3) using a constant value of n.

In the following, the error is estimated that occurs by the determination of the energy barrier ΔE_0 and H_0 by fitting $H(\ln(\kappa,t))$ data to Sharrock's equation. Equivalently, ΔE_0 and H_0 can be determined by fitting $\Delta E(H)$ with Eq. (3). The range used of the fit is $5k_BT_{300} < \Delta E(H) < 20k_BT_{300}$. The performance of the fit using Sharrock's equation is measured by comparing the extrapolated energy barrier at zero field as well as the extrapolated H_0 with the numerically calculated energy barrier and switching field. In Table I the performances of different fits using Sharrock's equation are compiled. The actual energy barrier at zero field is $85k_BT_{300}$. The external field is applied at an angle of 0.5° off the film normal. For a constant value of n=1.5 the extrapolated energy barriers show significant errors. For zero soft-layer thickness the energy barrier is underestimated by 18%. For a soft-layer thickness of 7 nm the energy barrier is overestimated by 8%. For the case of a large soft-layer thickness of 36 nm the

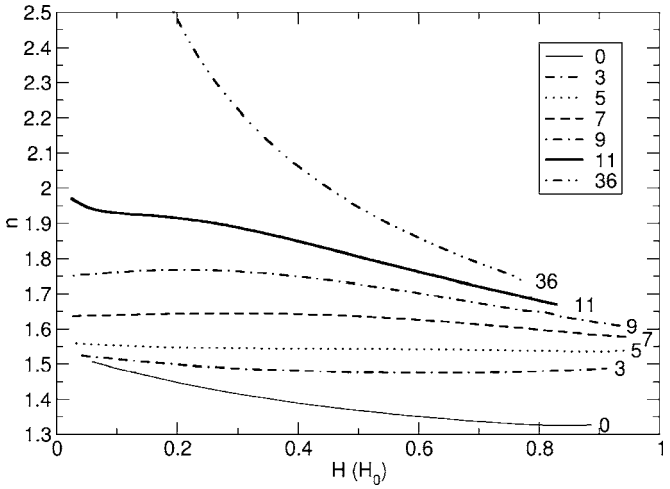

FIG. 7. Field dependence of the fitting parameter n. θ=45°. The hard-layer thickness t_h=18 nm. The numbers next to the curves denote the soft-layer thickness.

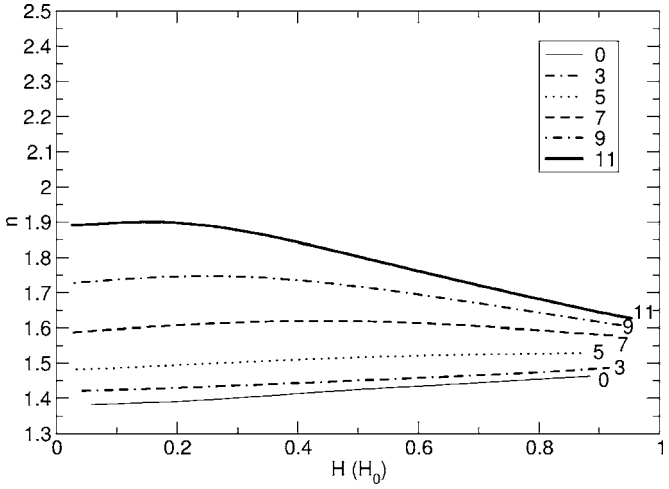

FIG. 8. Same as Fig. 3. However, t_h=10 nm.

largest error of an underestimation of about 40% occurs. Using the exponent n as an additional fit parameter the extrapolated energy barrier is even more inexact. Calculating the standard deviation of the error of the energy barrier for all investigated soft-layer thicknesses leads to $\sigma=12.72k_BT_{300}$ and $\sigma=9.47k_BT_{300}$ for using n as an additional fit parameter and a constant n of 1.5, respectively. In contrast to the energy barrier the extrapolation to determine H_0 is very good. The standard deviation of H_0 is just 0.03 T.

To summarize, E_0 cannot be extrapolated accurately for perpendicular recording media and exchange spring media from the dynamic coercivity (pulse duration is assumed to change from 10^{-7} s to about 1 s) if the field angle is close to the easy axis and a constant exponent n is assumed. This is an important fact because fitting the $\Delta E(H)$ loops of Fig. 4 with Eq. (3) in the whole range from $0 < \Delta E(H) < 85k_BT_{300}$ and using E_0, H_0, and n as free fit parameters leads to fits that do not seem too bad (solid lines in Fig. 4). Only for small energy barriers $\Delta E(H) \approx 5k_BT_{300}$ can clear misfits be observed.

In the following a method is presented that allows one to increase the accuracy of the measurement of the energy barrier of perpendicular recording media and exchange spring media. The origin of the wrong extrapolation of Sharrock's equation for exchange spring media can be found in the field dependence of the exponent n. The idea is to measure the energy barrier as a function of the applied field in such a way that $\Delta E(H)$ can be well described by Eq. (3). This can be realized as will be shown later by applying the field at a large angle of 45° with respect to the film normal.

In Fig. 6 the simulated energy barriers as a function of the external field are fitted with Eq. (3). The field angle is 45° with respect to the easy axis. For soft-layer thicknesses of 0–9 nm the fits are very good for the whole field range. The χ^2 values of the fits are 0.3, 0.02, 0.38, and 2 for soft-layer thickness of 3, 5, 7, and 9 nm, respectively. For very large soft-layer thicknesses the field dependence of the energy barrier can hardly be described with a simple power law. As shown in Fig. 6 for t_s=36 nm the fit is very bad, leading to a χ^2 value of 170.

In order to investigate the quality of the fit in more detail the exponent n is plotted as a function of the field strength H.

TABLE II. Same as Table I except that $\theta=45°$.

		Error $\mu_0 H_0$ (T)			Error ΔE ($k_B T_{300}$)		
t_s (nm)	n_{global}	Fit n	$n=1.5$	$n=n_{\text{global}}$	Fit n	$n=1.5$	$n=n_{\text{global}}$
0	1.39	**−0.02**	0.08	0.01	**−6.17**	8.17	−0.62
3	1.47	**−0.01**	0.00	0.00	**−0.31**	1.76	0.15
5	1.54	**0.00**	−0.01	0.00	**−0.48**	−2.33	0.06
7	1.68	**0.01**	−0.02	0.02	**−3.07**	−7.77	−1.66
9	1.85	**0.02**	−0.02	0.05	**−6.55**	−12.14	−2.87
11	2.04	**0.03**	−0.02	0.07	**−9.93**	−15.54	−5.45
Standard deviation		**0.02**	0.04	0.03	**3.80**	8.89	2.15

Figure 7 shows that for this field angle the exponent n only weakly depends on the strength of the external field for soft-layer thicknesses relevant for practical media in the range from 3 nm to 11 nm. Due to the insensitivity of n on H, the energy barrier as a function of the external field can be excellently fitted with Eq. (3).

This insensitivity of the exponent n on H for $\theta=45°$ also remains if other parameters of the exchange spring media such as the hard-layer thickness are changed as shown in Fig. 8. The thickness of the hard layer is 10 nm. The simulation for zero soft-layer thickness shows an exponent n that is in very good agreement with the Stoner-Wohlfarth theory. In general for different soft-layer thicknesses the exponent n is not 1.5 but varies from about 1.4 to about 2 depending on the actual sample. Since n mainly depends on the design of the particular exchange spring media, one can expect that n can be determined by using n as a free fit parameter in Sharrock's equation of using n as a fit parameter. If the accuracy of the vibrating sample magnetometer (VSM) measurement is not sufficient to use n as a free fit parameter, it might be possible to determine a global n by fitting results obtained using a contact tester, which can span many decades of time. For VSM measurements, modelers would need to suggest to experimentalists an appropriate n to use. The improved accuracy using n as a free fit parameter in the simulation could be confirmed as summarized in Table II. Measuring the remanent coercivity in a field range of $5k_BT_{300}<\Delta E(H)<20k_BT_{300}$ at an angle 45° and using n as a free fit parameter drastically increases the quality of the extrapolated energy barrier. The standard deviation of the error decreases to about $\sigma=2.8k_BT_{300}$.

Table III compiles the standard deviations of the error of the energy barrier and H_0 for the different measurements and different hard-layer thicknesses. For both $t_h=18$ nm and $t_h=10$ nm, the standard deviation of the error of ΔE_0 is about 3 times smaller than for the measurement with $\theta=0.5°$ and a constant value of $n=1.5$. Using n as a free fit parameter increases the quality of the fit only if n weakly depends on H, which is the case if the field is applied at an angle $\theta=45°$.

C. Exchange spring media with finite K_1 in the soft layer

In the previous sections the energy barrier was investigated for exchange spring media where the soft magnetic layer was perfectly soft. However, the assumption of a finite value of the anisotropy in the soft layer is more realistic. The shape anisotropy alone contributes considerably to the anisotropy of a granular grain with a large aspect ratio. Interestingly, a finite anisotropy in the soft layer is not only more realistic but also beneficial for magnetic recording because it further decreases the coercive field.[35] In Fig. 9, $\Delta E(H)$ is investigated for bilayers with a finite value of the anisotropy in the soft layer ($K_{1,\text{soft}}=2\times10^5$ J/m^3). The anisotropy in the hard layer is $K_{1,\text{hard}}=1\times10^6$ J/m^3. The hard layer thickness is 18 nm. The numbers in Fig. 9 denote the soft-layer thick-

TABLE III. Compilation of the standard deviations of the error in H_0 and ΔE for different exchange spring media. The standard deviation is calculated from data of six different soft-layer thicknesses as shown in Tables I and II. t_h is the hard-layer thickness of the bilayer.

		Error $\mu_0 H_0$ (T)			Error ΔE ($k_B T_{300}$)		
t_h (nm)	θ	Fit n	$n=1.5$	$n=n_{\text{global}}$	Fit n	$n=1.5$	$n=n_{\text{global}}$
10	0.5	0.06	**0.11**	0.04	9.98	**9.24**	2.68
10	5.0	0.04	**0.03**	0.03	6.09	**6.30**	1.74
10	45.0	**0.02**	0.02	0.04	**3.86**	6.78	2.39
18	0.5	0.04	**0.03**	0.09	12.72	**9.47**	3.96
18	5.0	0.04	**0.06**	0.07	8.94	**6.55**	2.28
18	45.0	**0.02**	0.04	0.03	**3.80**	8.89	2.15

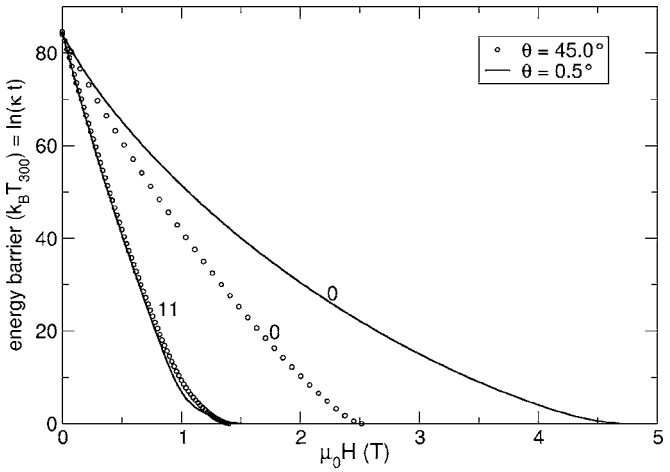

FIG. 9. Energy barrier of exchange spring media for different soft-layer thicknesses and different angles θ between the external field and the easy axis. The anisotropy constant in the hard layer and in the soft layer is $K_{1,\mathrm{hard}}=1\times10^6$ J/m^3 and $K_{1,\mathrm{soft}}=2\times10^5$ J/m^3, respectively. The numbers in the figure denote the soft-layer thicknesses.

nesses. It is interesting to note that for a soft-layer thickness of 11 nm, H_0 for $\theta=0.5°$ is similar to H_0 for $\theta=45°$. This is in contrast to the Stoner-Wohlfarth theory, which predicts a minimum of H_0 at $\theta=45°$. This effect is also in contrast to the predictions of a pure pinning behavior, where the coercive field follows $H_0\propto 1/\cos(\theta)$ according to Kondorsky.[36]

The observed angular dependence of H_0 is summarized in the inset of Fig. 10. The angular dependence can be understood if one keeps in mind that the reversal process in exchange spring media occurs in two steps. In a first step a nucleation is formed into the soft layer. This nucleation process shows an angular dependence similar to the prediction of the Stoner-Wohlfarth theory, $H_N\propto[\sin^{2/3}(\theta)+\cos^{2/3}(\theta)]^{-3/2}$.

In a second step the domain wall that was nucleated propagates towards the soft-hard interface. The angular dependence of the (pinning) field to push the domain wall in the hard layer follows $H_P\propto 1/\cos(\theta)$. The switching field H_0 is determined by $H_0=\max(H_N,H_P)$. Since the nucleation field and the pinning field show a different angular dependence, it may depend on the angle θ if the switching field is determined by H_N or by H_P. In the investigated sample the angular dependence of $H_0(\theta)$ follows a Stoner-Wohlfarth-like behavior for small angles θ. For larger angles the nucleation field becomes smaller than the pinning field. Hence for large angles the switching field $H_0(\theta)$ is determined by H_P, leading to pinninglike behavior $H_0\propto 1/\cos(\theta)$. In Fig. 11 the exponent n is calculated by fitting $\Delta E(H)$ data to Eq. (3). Similar to the results for a perfectly soft layer, the exponent n strongly depends on the applied field strength for $\theta=0.5°$. Even values of n larger than 2 are observed. Similar to the results of the last section, the exponent n becomes less dependent on H if the external field is applied at an angle $\theta=45°$ (see Fig. 12). Values close to $n=3/2$ are observed. To find a physical argument that explains why for a variety of samples the exponent n becomes almost constant if the angle is applied at 45° will be a task of future research.

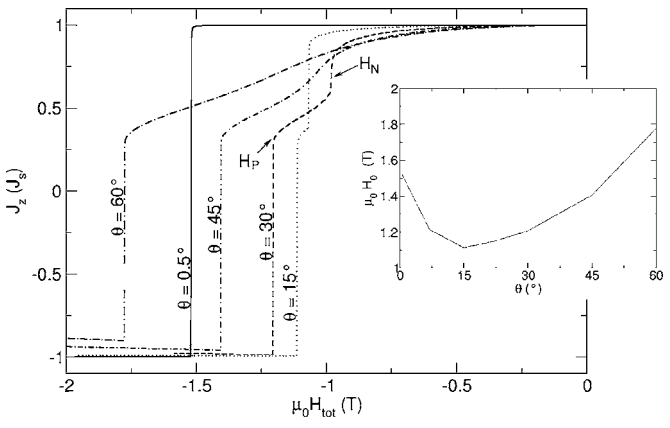

FIG. 10. Hysteresis loops of a bilayer with an 18-nm-thick hard layer and an 11-nm-thick soft layer ($K_{1,\mathrm{hard}}=10^6$ J/m^3, $K_{1,\mathrm{soft}}=2\times10^5$ J/m^3). The angle θ between the external field and the easy axis is varied. The inset shows the angular dependence of H_0 as a function θ.

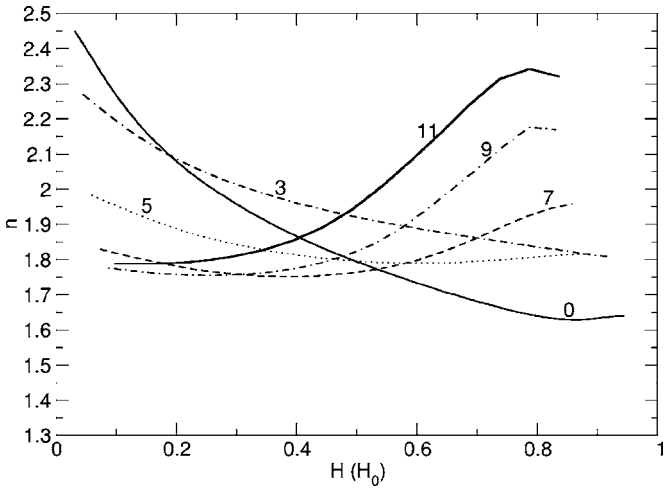

FIG. 11. Same as Fig. 5 ($\theta=0.5°$, $t_h=18$ nm). However, the anisotropy in the soft layer is $K_1=2\times10^5$ J/m^3.

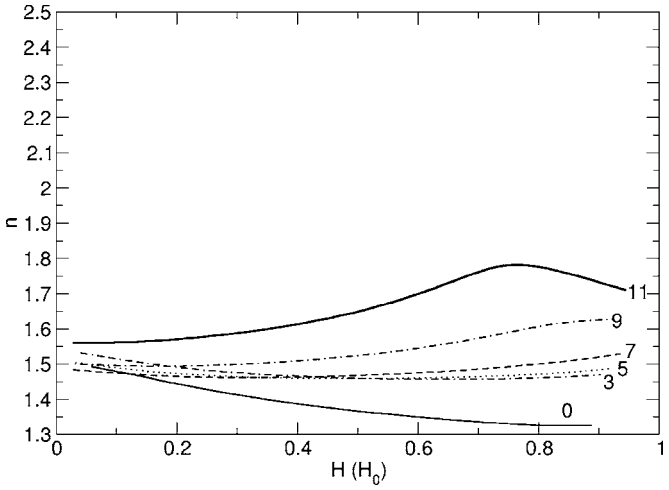

FIG. 12. Same as Fig. 11 except that $\theta=45°$.

V. CONCLUSION AND OUTLOOK

Monte Carlo simulations of dynamic coercivity simulations have shown that the interaction fields such as the exchange field and the strayfield do not significantly change the dynamic coercivity. Although Sharrock's equation was derived without taking interaction fields into account, it is well suited to describe interacting grains of magnetic structures.

The analysis of the paper shows that the accuracy of measurements of energy barriers of exchange spring media can be improved by changing the experimental conditions. We propose that the external field is applied at 45° with respect to the film normal. For measurements under 45° the exponent n is almost constant which is in contrast to measurement parallel to the film normal. This makes it possible to use n as an additional fit parameter along with the fitted energy barrier at zero field ΔE_0 and the fitted H_0.

ACKNOWLEDGMENTS

The financial support of the Austrian Science Fund P19350 is acknowledged. I would like to thank P. Visscher for helpful discussions.

*Electronic address: dieter.suess@tuwien.ac.at

[1] E. E. Fullerton, D. T. Margulies, M. E. Schabes, M. Carey, B. Gurney, A. Moser, M. Best, G. Zeltzer, K. Rubin, H. Rosen, and M. Doerner, Appl. Phys. Lett. **77**, 3806 (2000).
[2] E. N. Abarra, A. Inomata, H. Sato, I. Okamoto, and Y. Mizoshita, Appl. Phys. Lett. **77**, 2581 (2000).
[3] M. P. Sharrock, J. Appl. Phys. **76**, 6413 (1994).
[4] D. T. Margulies, A. Berger, A. Moser, M. Schabes, and E. Fullerton, Appl. Phys. Lett. **82**, 3701 (2003).
[5] R. Coehoorn, D. B. de Mooij, and C. de Waard, J. Magn. Magn. Mater. **80**, 101 (1989).
[6] E. F. Kneller and R. Harwig, IEEE Trans. Magn. **27**, 3588 (1991).
[7] T. Schrefl, H. Kronmüller, and J. Fidler, J. Magn. Magn. Mater. **127**, L273 (1993).
[8] K. Mibu, T. Nagahama, and T. Shinjo, J. Magn. Magn. Mater. **163**, 75 (1989).
[9] E. E. Fullerton, J. S. Jiang, M. Grimsditch, C. H. Sowers, and S. D. Bader, Phys. Rev. B **58**, 12193 (1998).
[10] R. H. Victora and X. Shen, IEEE Trans. Magn. **41**, 2828 (2005).
[11] D. Suess, T. Schrefl, R. Dittrich, M. Kirschner, F. Dorfbauer, G. Hrkac, and J. Fidler, J. Magn. Magn. Mater. **290-291**, 551 (2005).
[12] J. P. Wang, W. K. Shen, and J. M. Bai, IEEE Trans. Magn. **41**, 3181 (2005).
[13] N. Supper, D. T. Margulies, A. Moser, A. Berger, H. Do, and Eric E. Fullerton, IEEE Trans. Magn. **41**, 3238 (2005).
[14] F. Garcia-Sanchez, O. Chubykalo-Fesenko, O. Mryasov, R. W. Chantrell, and K. Y. Guslienko, Appl. Phys. Lett. **87**, 122501 (2005).
[15] S. Mukherjee and L. Berger, J. Appl. Phys. **99**, 08Q909 (2006).
[16] A. Dobin and J. Richter, Appl. Phys. Lett. **89**, 062512 (2006).
[17] D. Suess, J. Magn. Magn. Mater. **308**, 183 (2007).
[18] D. Suess, Appl. Phys. Lett. **89**, 113105 (2006).
[19] D. Givord and M. F. Rossignol, in *Rare-Earth Iron Permanent Magnets*, edited by J. M. D. Coey (Oxford University Press, Oxford, 1996), p. 218.
[20] R. Victora, Phys. Rev. Lett. **63**, 457 (1989).
[21] J. W. Harrell, IEEE Trans. Magn. **37**, 533 (2001).
[22] Z. G. Zhang, K. G. Kang, and T. Suzuki, IEEE Trans. Magn. **40**, 2455 (2004).
[23] V. G. Voznyuk, A. Misra, W. D. Doyle, and P. Visscher, IEEE Trans. Magn. **40**, 2501 (2004).
[24] W. Scholz, T. Schrefl, and J. Fidler, J. Magn. Magn. Mater. **233**, 296 (2001).
[25] J. L. Garcia-Palacios and F. J. Lazaro, Phys. Rev. B **58**, 14937 (1998).
[26] G. Henkelman and H. Jónsson, J. Chem. Phys. **113**, 9978 (2000).
[27] R. Dittrich, T. Schrefl, D. Suess, W. Scholz, H. Forster, and J. Fidler, J. Magn. Magn. Mater. **250**, 12 (2002).
[28] A. Bortz, M. Kalos, and J. L. Liebowitz, J. Comput. Phys. **17**, 10 (1975).
[29] S. H. Charap, P. L. Lu, and Y. J. He, IEEE Trans. Magn. **33**, 978 (1997).
[30] R. W. Chantrell, N. Walmsley, J. Gore, and M. Maylin, Phys. Rev. B **63**, 024410 (2000).
[31] H. Pfeiffer, Phys. Status Solidi A **118**, 295 (1990).
[32] H. J. Richter, IEEE Trans. Magn. **29**, 21 (1993).
[33] X. W. Wu, H. Zhou, D. Weller, and H. J. Richter, J. Magn. Magn. Mater. **303**, 5 (2006).
[34] P. Loxley and R. L. Stamps, IEEE Trans. Magn. **37**, 1998 (2001).
[35] F. B. Hagedorn, J. Appl. Phys. **41**, 2491 (1970).
[36] E. Kondorsky, J. Phys. (Moscow) **11**, 161 (1940).